sustainability

MDPI

Article

Prediction of the Water Inrush Risk from an Overlying Separation Layer in the Thick Overburden of a Thick Coal Seam

Daolei Xie [1], Zhongwen Du [1], Chenghao Han [2,*], Jie Han [3], Jiuchuan Wei [1] and Jiulei Yan [4]

[1] College of Earth Science and Engineering, Shandong University of Science and Technology, Qingdao 266590, China; skd994469@sdust.edu.cn (D.X.); yjsdzw@163.com (Z.D.); jcwee@126.com (J.W.)
[2] College of Energy and Mining Engineering, Shandong University of Science and Technology, Qingdao 266590, China
[3] Yankuang Energy (Ordos) Co., Ltd., Ordos 017010, China; yjssdust@163.com
[4] Shandong Energy Group Luxi Mining Co., Ltd., Heze 274700, China; yjlsdust@163.com
* Correspondence: sdusthch@163.com

Abstract: With the expansion of coal mining westward in China, water inrush from seam roofs has become a prominent safety problem during mining. The roof rock of the coal seam in the Shilawusu coal mine has the characteristics of a double-layer structure, and the overlying separation space formed in the mining process of the coal seam poses a risk of water inrush. To ensure the safety of coal mine production, considering the geological and hydrogeological data of the mining area, the core recovery rate, lithologic assemblage index, key aquifer thickness, hydrostatic head and lithologic structure index of the Zhidan Formation are selected as evaluation indexes. The index weights are calculated based on the attribute hierarchical model and coefficient of variation methods, and subjective and objective preference coefficients are introduced to determine the ranking of comprehensive indexes. The catastrophe progression method is improved, and a zoning prediction model for water inrush risk is established by the improved catastrophe progression method. The results show that only a tiny part of the mining area is in danger, and most areas are in the safe and transition zones. The model realizes the prediction of the risk of water inrush from the overlying separation layer in the study area and provides a theoretical basis for the prevention and control of water inrush from the overlying separation layer in coal mining.

Keywords: attribute hierarchical model; coefficient of variation method; improved catastrophe progression method; risk of water inrush

Citation: Xie, D.; Du, Z.; Han, C.; Han, J.; Wei, J.; Yan, J. Prediction of the Water Inrush Risk from an Overlying Separation Layer in the Thick Overburden of a Thick Coal Seam. *Sustainability* **2023**, *15*, 13988. https://doi.org/10.3390/su151813988

Academic Editor: Cun Zhang

Received: 2 August 2023
Revised: 13 September 2023
Accepted: 18 September 2023
Published: 20 September 2023

1. Introduction

The Shaanxi and Mongolia region in Western China is an important coal base in China and plays a pivotal role in energy cooperation along the "Belt and Road Initiative" route and in the construction of national energy transportation channels. However, in 2006, secondary water from bed separation occurred in the 745 workfaces of Haizi coal mine, with an inflow of 3887 m^3/h, resulting in the death of five workers [1]. On 25 April 2016, the ZF202 working face of Zhaojin coal mine in Tongchuan caused many deaths due to the increasing volume of space between layers of overlying strata and water that had accumulated in the space [2]. When the mining face in the Hongliu coal mine advanced different distances from the initial cut, the maximum water inflow increased to 3000 m^3/h [3]. Therefore, the threat of water inrush from an overlying separation layer has been given increasingly more attention in mining engineering. It is significant to accurately predict the risk of water inrush from the overlying separation layer for the safety of coal mine production. Due to the excellent occurrence state of the coal seams in the northern Ordos Basin, the coal seam roof can be described as a double-layer structure with a coal-measure composite aquifer and Cretaceous Zhidan Formation aquifer, which indicates that the coal mining in this region will face the threat of water inrush from separated layers. As a newly identified type of roof

water hazard, water inrush from layer separation can influence the average production of coal mines and the safety of personnel underground. Therefore, it is significant to accurately predict the risk of water inrush from an overlying separation layer for coal mine safety and production.

At present, many experts and scholars focus on the location of the separation layer water damage and the mechanism of water inrush from the separation layer and have achieved substantial results. Qiao et al. [4] summarized the main theories to explain and judge the development of overburden separation in China, including key layer theory, arch beam balance theory, "upper four belts" theory and elastic thin plate theory. Gui et al. [5] analyzed the key influencing factors of the formation of a separation layer and the occurrence of water disasters and provided a reference for further research on water inrush and disaster prevention in coal mines. Yan et al. [6] proposed a new method to predict the location of roof strata separation and derived the calculation formula of bedding separation in roof strata by combining the theoretical analysis and test results of continuous and discontinuous beams and layered strata loads. He et al. [7] proposed an improved stepwise comparative combination method based on composite beam theory to determine the location of a separation layer. According to key strata theory, Hu et al. [8] determined the position of separated beds in overlying rocks and introduced the trapezoidal platform model of the cracks in overlying strata. Ji et al. [9] studied the mechanism of four large water inrush events in the mining process of the Hongliu coal mine 1121 workface in the Ningdong mining area. Wu et al. [10] used the rock plate method to study the deformation and internal force of coal seam roofs and proposed an identification method for isolated water damage. Gui et al. [11] studied the restriction effect of geological and mining factors such as roof rock lithology, coal seam dip angle, separation layer water source, roof management mode, working face size and mining schedule on the formation of water damage to the separation layer. Numerical simulation and physical simulation also play an important role in the study of separation layers. Li et al. [3] studied the evolution of water inrush through numerical simulation and underground full-space transient electromagnetic detection and concluded that water inrush from a separation layer is due to unique geological conditions, lithology and mining conditions. Gui et al. [12] determined the location of the separation layers and the location of the most dangerous separation layer of the overlying strata through numerical simulation and similar material simulation. Wang et al. [13] developed a new type of similar material to simulate the separation of rock layers and observe the water flow in the waterproof layer. Wang et al. [14] experimentally revealed the evolution of layer separation, the process of water accumulation due to layer separation and the damage characteristics of water inrush due to layer separation. By means of numerical simulation and analysis, Li et al. [15] studied the influencing factors and mechanism of water inrush from the separation layer and proposed effective measures for the prevention and control of separation layer water inrush. In addition, the risk assessment system of water inrush of coal seams tends to be mature in China [16–22].

The above work has carried out a series of theoretical studies on the formation of the conventional separation layer and the mechanism of water inrush from the separation layer. However, coal seam occurrence conditions are relatively good in China's northern mining area of the Ordos Basin. The coal seam roof can be divided into a double-layer structure, which includes a coal-measure composite aquifer and the Cretaceous Zhidan Formation aquifer. There are few studies on the prediction of water inrush of high separation layer water, which seriously threatens the safety of mine mining. Therefore, this paper establishes a more comprehensive and objective risk prediction model that combines subjective and objective weights with the catastrophe progression method. The risk of water inrush from the separation layer in the 221 mining area of Shilawusu coal mine is predicted, and the evaluation results have important guiding significance for the mining area in the north of Ordos Basin.

2. Materials and Methods

2.1. Geological Setting

The Dongsheng coal field, Shilawusu coal mine, is located in Ordos city, and the administrative division is under the jurisdiction of the Ejin Horo Banner of Ordos city. The length of the coal mine is 7.35 km from north to south and 9.40 km from east to west on average, covering an area of 70.644 km^2 (Figure 1). The coal seam is adjacent to the Hulusu well field to the west and the No. 2 exploration area to the south. Strata in the area include, from old to young, the upper Triassic Yanchang Formation (T_3y), middle–lower Jurassic Yan'an Formation ($J_{1-2}y$), middle Jurassic Zhiluo Formation (J_2z), middle Jurassic Anding Formation (J_2a), lower Cretaceous Zhidan Formation (K_1zh), upper Quaternary Pleurian Malan Formation (Q_3m), Quaternary Holocene Aeolian Layer (Q_4eol) and alluvial sand (Q_{4al+pl}); see Table 1 for a brief list of stratum characteristics in the mining area.

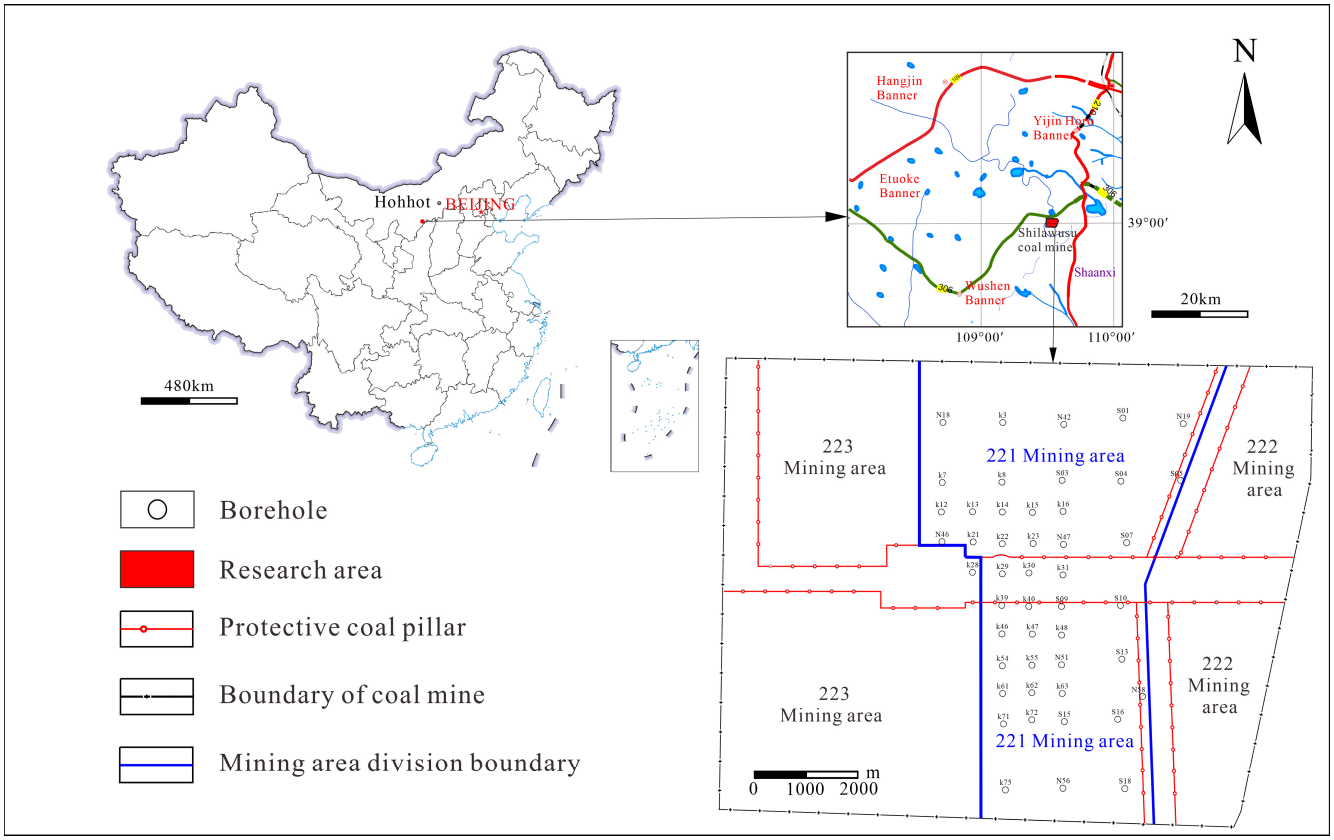

Figure 1. Location map of the study area.

Table 1. Summary table of regional stratigraphic characteristics.

Era	System	Series	Formation	Thickness (m)	Lithologic Description
Cenozoic	Quaternary	Holocene	Alluvial sand (Q_{4al+pl})	<200	Light yellow–brown, yellow medium fine sand and silty sand. Lacustrine sedimentary layer, alluvial–diluvium layer and eolian layer.
			Aeolian layer (Q_4eol)		Brown gravel, grayish yellow sand and silty sand. The thickness of sand layer in the western desert is 0~180 m.
		Upper Pleistocene	Malan Formation (Q_3m)	0~40	Yellowish sandy loess with calcareous nodules, columnar joints, unconformable above all older strata.

Table 1. *Cont.*

Mesozoic	Cretaceous	Lower	Zhidan Formation (K_1zh)	40~230	The upper part is light gray, gray–purple, gray–yellow, yellow, purple and red mudstone, siltstone, fine sandstone, sand conglomerate mudstone sand mudstone interbedded with thin layers of argillaceous limestone. Cross-bedding is more developed. Large cross-bedding and channel migration are common at the bottom. Unconformable contact with the underlying floor.
				30~280	The lower part is light gray, gray–green, brown, red, gray, and purple mudstone, siltstone, sandy mudstone and various grained sandstones and conglomerates, with thin layers of calcareous fine sandstone. Argillaceous cement, relatively loose, with oblique bedding development. Large cross-bedding is common at the bottom. Unconformable contact with the underlying floor.
	Jurassic	Middle	Anding Formation (J_2a)	10~151	Light gray, gray–green, yellow, purple and brown mudstone, sandy mudstone, medium sandstone. Calcareous nodules and argillaceous masses with parallel bedding and cross bedding.
			Zhiluo Formation (J_2z)	10~400	Gray, gray–yellow, gray–green and purplish red mudstone, sandy mudstone, fine sandstone, medium sandstone and coarse sandstone, with cross-bedding and wavy bedding. The lower part sandwiches a thin coal seam and oil shale, containing the 1 coal group. Coal bearing layers 1~3. Pseudoconformity contact with the underlying floor.
		Lower	Yan'an Formation ($J_{1-2}y$)	78~458	The sandstones of various gray–gray to grayish white grade are interbedded with dark gray and grayish black sandy mudstone and mudstone. Including coal seams with industrial mining value. Contains the 2, 3, 4, 5, 6, 7 coal groups, 27 layers of coal; among them, the main recoverable coal seams are 2-2 middle, 3-1, 4-1, 4-2 middle, 5-1, 6-1 middle, 6-2. Conformable contact with the underlying floor
	Triassic	Upper	Yanchang Formation (T_3y)	35~312	Gray–green, yellow, purple, gray–black massive coarse and medium sandstone, local containing fine gravel, mudstone, siltstone and coal line. Pseudoconformity contact with the underlying floor.

This paper selects the 221 mining area, which is located in the middle of the Shilawusu coal mine, as the study area. The 221 mining area is approximately 7.4 km from north to south and 5.1 km from east to west, covering an area of 37.74 km^2. The main coal-bearing strata are the Yan'an Formation ($J_{1-2}y$) of the middle Lower Jurassic, with no surface outcrop and stable coal seam deposition. The main coal seam is 2-2 coal seam, and the coal thickness is approximately 9.18 m. The base of the coal seam is the Yanchang Formation of the upper Triassic system.

In the study area, the middle and upper parts of the Yan'an Formation, Zhiluo Formation and Anding Formation are interbedded with sandy mudstone and sandstone (59.3% sandstone on average). Coal measures are dominated by aquifers. The rock beam combination is mainly composed of coarse sandstone, medium sandstone and fine sandstone, and the rocking beam overlying rock is generally a secondary-grained rock layer. The rock beam combination is relatively complex, and the mechanical properties of rock

strata in this group are more obvious than those in the Zhidan Formation. The overall water richness is weak.

Here, the Cretaceous system is mainly the lower Cretaceous Zhidan Formation strata. The lithology is dominated by fine sandstone, medium sandstone and coarse sandstone (90% sandstone), and sandy mudstone and mudstone are rarely developed (Table 2). The rock beam is mainly composed of thick, gravelly strata and the combined structure of the rock beam is more straightforward compared to the coal-measure composite aquifer. The brittleness characteristic of mechanical properties is relatively apparent, and the overall water richness is high.

Table 2. Lithologic statistics.

Stratum / Lithology	$J_{1-2}y$		J_2z		J_2a		K_1zh	
	Average Thickness (m)	Proportion (%)	Average Thickness (m)	Proportion (%)	Average Thickness (m)	Proportion (%)	Average Thickness (m)	Proportion (%)
Coarse Sandstone	3.58	7	9.07	11	11.98	7	26.86	8
Medium Sandstone	10.65	21	14.67	17	19.51	12	86.51	25
Fine Sandstone	13.31	26	15.9	19	31.45	19	142.92	42
Siltstone	6.59	13	10.67	12	22.75	14	50.59	15
Mudstone	16.92	33	35.06	41	79.73	48	34.23	10

Based on the above differences above the roof of the coal seam in the study area, the whole stratum in the study area is divided into a double-layer structure (Figure 2), that is, from the bottom to top of the 2–2 coal roof of the main coal seam, two combined water-bearing rock groups can be distinguished: the first layer of the coal-measure composite aquifer and the second layer of the Cretaceous Zhidan Formation aquifer.

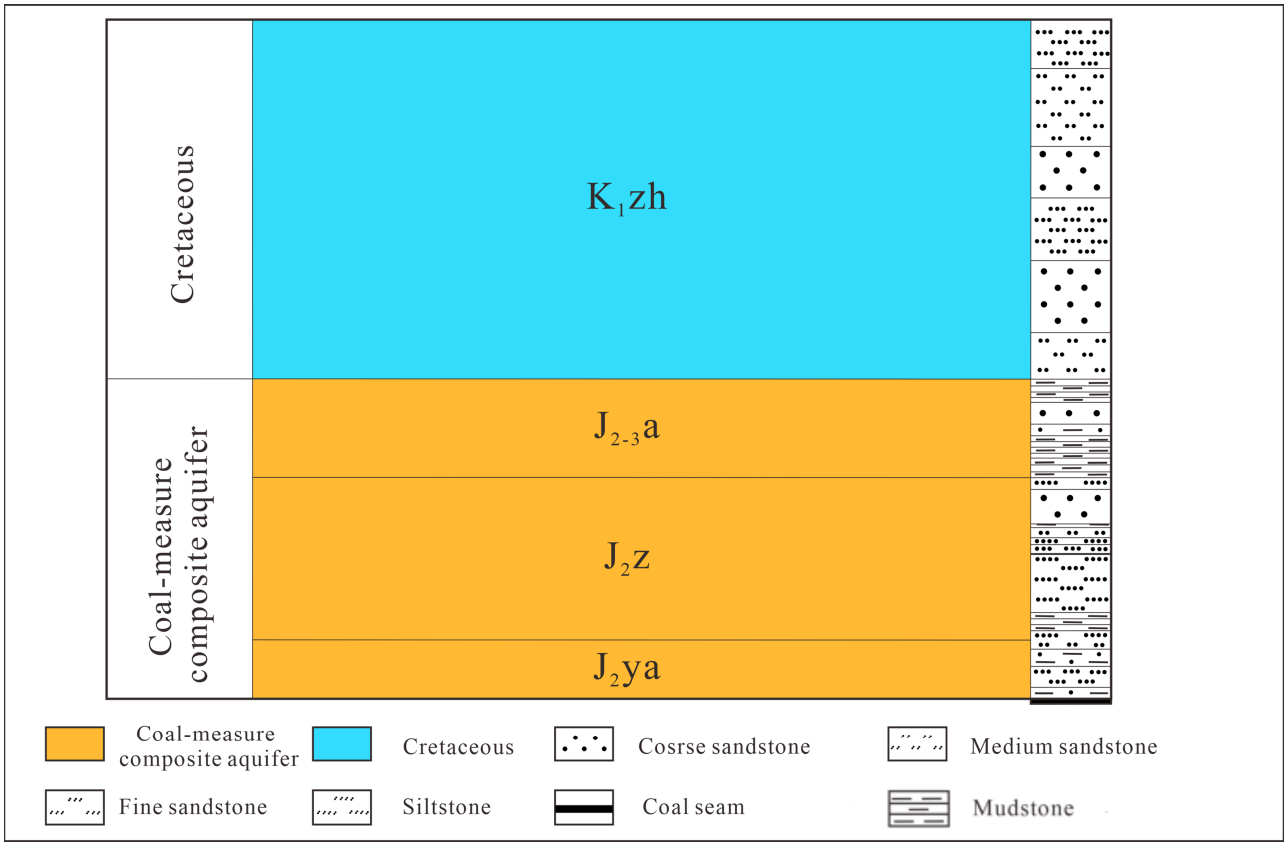

Figure 2. Schematic diagram of double–layer structure.

2.2. Evaluation Model and Weight Determination Method

As the workface advances, different mechanical properties, different degrees of softness and hardness of the rock layer and the interlayer cohesion will cause the lower rock layer under the action of self–weight on the upper rock layer to produce tensile force. When the tensile force reaches the limit of interlayer tensile strength, the upper and lower layers of the rock layer is separated, resulting in the occurrence of varying degrees of subsidence and their independent bending and deformation [23]. When the tensile force reaches the ultimate tensile strength between layers, the upper and lower rock layers are separated, different degrees of settlement occur, and they independently bend. When the deformation reaches a certain degree, a separation space is formed between the soft and hard rock layers. Water inrush is likely to cause a disaster when the following four conditions are met: a closed and sustainable separation space, a water replenishment channel, a stable water source and a water inrush channel.

Under the condition of double-layer overlying rock, the mining of deep and thick coal seams results in the development of large–scale layer separation between the double-layer overlying coal measures and the Cretaceous series on the basis of the traditional "upper three zones". With the continuous mining of the lower coal seam, the range of the overlying separation continues to expand. However, due to the weak cementation and brittle deformation characteristics of the upper overburden of the separated roof, new fracture movement occurs within a certain range of the overburden, namely the secondary movement (Figure 3). The intensity and scale of the movement of the extremely thick sandstone layer in the overlying Zhidan Formation are both large due to secondary movement. The deformation is no longer the fracture and bending of the rock layer in a single layer or small range, but is instead the fracture of a group of strata. The bottom rock layer of the Zhidan Formation is broken, the upper rock layer is curved, and a separation space is generated. When the aquiclude at the lower part of the separation layer breaks under the double action of mine pressure and water pressure, the water in the separation layer will flow into the working face and cause a water inrush accident (Figure 4).

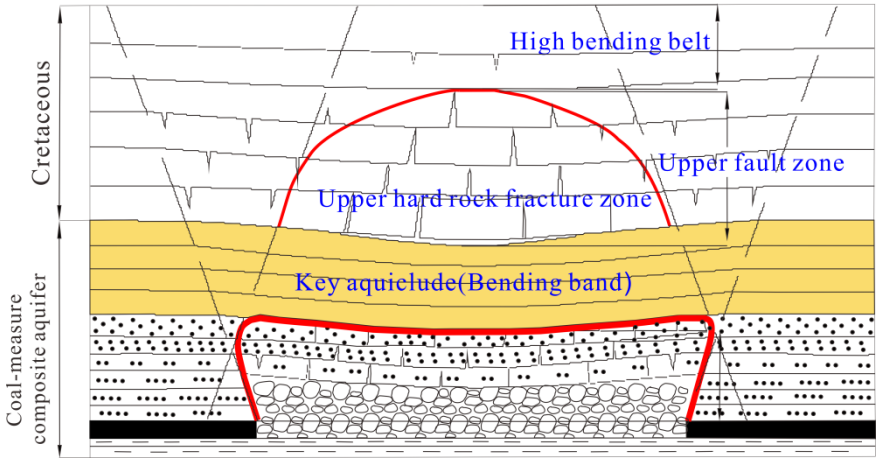

Figure 3. Schematic diagram of secondary movement of double-layer structure overlying strata.

The possibility of water inrush is closely related to the key aquiclude and the properties of the underlying barrier layer for the overlying separation layer containing confined water. Therefore, in view of the double-layer structure characteristics of overburden strata of the 2-2 coal seam in the 221 mining area, this paper selects five indexes, namely, core recovery rate of the key aquiclude, lithologic assemblage index of the key aquiclude, thickness of the key aquiclude, static pressure head and lithologic structure index of the Zhidan Formation, as the basis for studying water inrush from an overlying separation layer of a coal seam roof.

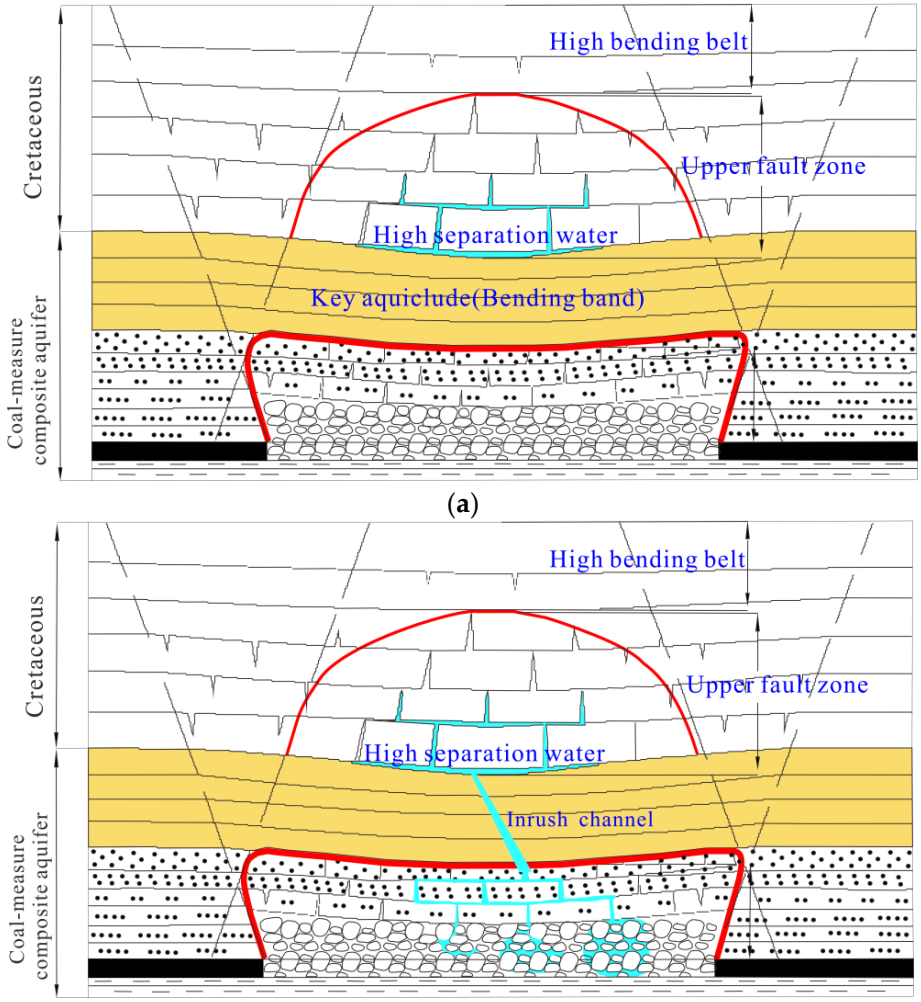

Figure 4. The formation process of the separation layer water hazard: (**a**) Formation of an overlying separation layer water; (**b**) Outburst of the separated water body.

2.2.1. Core Recovery Rate of the Key Aquiclude (C_1)

The core recovery rate refers to the ratio of the length of the core recovered to the length drilled in the drilling process, which can reflect the fragmentation degree of the stratum to a certain extent [24]. The larger the core recovery rate is, the more complete the rock mass, the less developed the cracks and the stronger the water insulation performance. In contrast, the water insulation performance is weaker, the water permeability and conductivity are stronger and the corresponding water insulation performance is worse for smaller core recovery rates. Therefore, the core recovery rate of the key aquiclude is negatively correlated with the risk of water damage from upper layers (Figure 5).

2.2.2. Lithologic Assemblage Index of Key Aquiclude (C_2)

A large number of studies have shown that the unit water inflow in lithologic assemblages is generally larger if the proportion of sandstone is larger, while the unit water inflow in lithologic assemblages is smaller if the proportion of sandstone is smaller. It is generally believed that as the proportion of sandstone decreases, the porosity will gradually decrease, so the capacity of water storage and water conduction will gradually decrease, and then the aquiclude performance will gradually strengthen. Therefore, different structural coefficients can be assigned to different rock types (Table 3). The larger the structural coefficient is, the larger the particle size of the rock, and thus the poorer the barrier performance of the rock. Hou et al. [25] proposed the lithologic assemblage of key aquifers as an

evaluation index of waterproofing. Therefore, in this paper, the thicknesses and structural coefficients of different lithologies in the key aquiclude are used to construct the lithologic assemblage index z, reflecting the key aquiclude to evaluate the key aquiclude performance (Equation (1)).

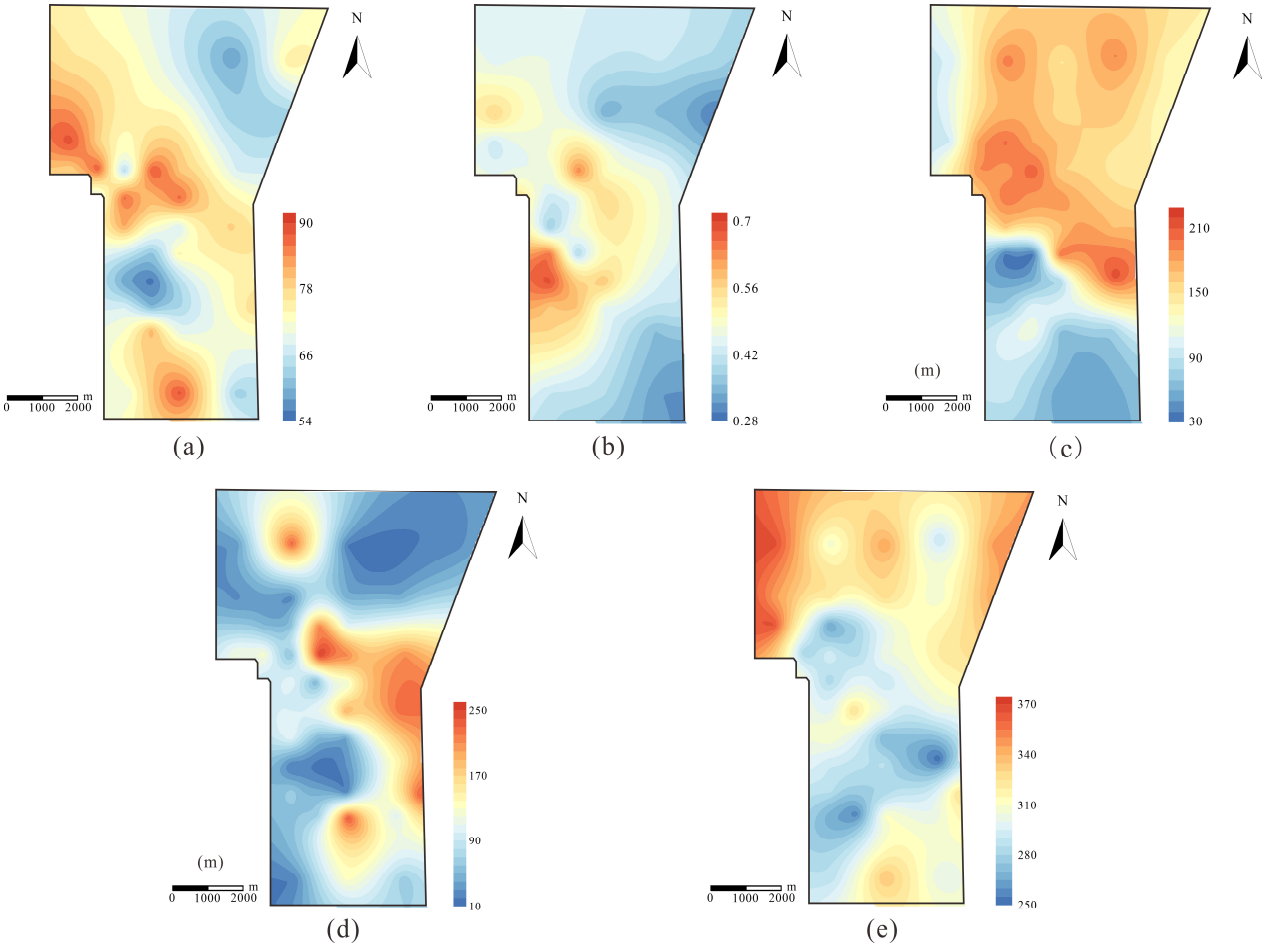

Figure 5. Thematic maps of each main controlling factor. (**a**) Core recovery rate in key aquiclude. (**b**) Lithologic assemblage index of key aquiclude. (**c**) Key aquiclude thickness. (**d**) Lithologic structure index of the Zhidan Formation. (**e**) Hydrostatic head.

Table 3. Structural coefficient table.

Rock Types	Coarse Sandstone	Medium Sandstone	Fine Sandstone	Siltstone	Sand Mudstone	Mudstone
Structural coefficient	1	0.8	0.6	0.4	0.3	0.2

$$z = \frac{\sum hisi}{\sum hi} (i = 1, 2 \ldots, 6) \quad (1)$$

where h_i represents the thickness of coarse sandstone, medium sandstone, fine sandstone, siltstone, sandy mudstone and mudstone for i = 1, 2, 3, 4, 5 and 6, respectively, and S_i is the corresponding structural coefficient.

The larger the z value is, the larger the proportion of sandstone in the key waterproof layer, the better the water storage and water conductivity, and the lower the aquiclude performance; in contrast, the larger the z value is, the stronger the water resistance. Therefore, the lithologic assemblage index of the key aquiclude is positively correlated with the risk of water damage from the upper layers.

2.2.3. Key Aquiclude Thickness (C_3)

The thickness of the key aquiclude is an important factor affecting water inrush from overlying separation layers. The greater the thickness of the key aquiclude, the stronger the ability to resist water pressure in overlying separation layers, the lower the possibility of connecting a water channel below the separation layers to the lower key separation layer and the lower the risk of water inrush in the overlying separation layers. Therefore, the thickness of the key aquiclude is negatively correlated with the risk of water damage from upper layers.

2.2.4. Lithologic Structure Index of the Zhidan Formation (C_4)

The lithologic structure index is used to multiply the thickness of the aquifer in the Zhidan Formation, including the thicknesses of the medium sandstone and fine sandstone by an equivalent coefficient, and then convert it into the thickness of coarse sandstone. Considering the number of alternating sandstone–mudstone layers, the more mudstone–mudstone (siltstone) interlayer combinations there are, the weaker the water-carrying performance, so the number of sandstone–mudstone interlayers is negatively correlated with S when other conditions remain unchanged.

The water-richness of the Zhidan Formation sandstone aquifer, as the main aquifer of the overlying separation layer cavity, will affect the outburst risk of overlying separation layer water. The greater the water-richness, the greater the water volume and the greater the outburst risk of overlying separation layer water. In contrast, the lower the water-richness, the lower the water outburst risk of overlying separation layer water. Therefore, the lithologic structure index of the Zhidan Formation is positively correlated with the risk of water damage in the upper strata.

Based on the above analysis, the expression of the lithologic structure index was constructed as follows:

$$S = \frac{(a + b \times i + c \times j)}{n} \quad (2)$$

where a, b and c are the thicknesses of the coarse sandstone, medium sandstone and fine sandstone, respectively; m, and i and j are the equivalent coefficients of the medium sandstone and fine sandstone, respectively; and n is the number of sandstone–mudstone (siltstone) interbeds.

2.2.5. Hydrostatic Head (C_5)

There are many unexploited areas in the mining area, so the highest water level of the sandstone aquifer of the Zhidan Formation in the mining area is used as its head elevation. The higher the water head in the overlying separation area, the greater the water pressure, and the more likely the water is to surge into the lower channel fracture zone, resulting in the risk of water damage; otherwise, the risk of water inrush is smaller. Therefore, the hydrostatic water head of the sandstone aquifer in the Zhidan Formation is positively correlated with the risk of water damage to upper layers. The elevation of the sandstone aquifer floor in the Zhidan Formation was calculated using the borehole data in the mining area, and then the static pressure head at the overlying separation space was calculated.

2.2.6. Data Statistics

According to risk factor analysis, 47 boreholes in the 221 mining area were selected for statistical analysis, and the original data are shown in Table 4.

Table 4. Statistical table of risk assessment indexes.

Borehole	C_1 (%)	C_2	C_3 (m)	C_4 (m)	C_5 (m)
S01	58.19	0.43	191.93	18.42	288.85
S03	73.50	0.34	155.51	43.91	328.60
S04	62.50	0.36	166.46	43.14	306.08
S05	63.20	0.30	128.26	71.37	344.27
S07	67.57	0.46	142.90	208.82	322.35
S09	67.67	0.54	166.33	192.63	304.54
S10	78.44	0.48	169.33	226.25	302.72
S13	74.00	0.45	216.74	148.59	250.50
S15	69.20	0.45	63.54	240.85	311.26
S16	70.80	0.36	74.53	104.20	300.87
S18	63.20	0.32	57.45	63.94	299.67
N18	76.43	0.45	103.80	34.03	366.79
N42	67.00	0.42	148.35	18.66	345.27
N19	75.50	0.39	133.64	26.23	347.56
N46	78.71	0.45	137.05	121.11	335.24
N47	79.50	0.50	159.67	212.97	304.54
N51	64.75	0.58	79.52	29.18	286.04
N56	89.00	0.40	52.15	133.88	335.96
N58	77.17	0.42	139.53	233.49	324.82
k3	74.12	0.46	195.89	230.67	306.67
k7	84.75	0.56	111.40	28.12	346.17
k8	74.71	0.48	176.50	24.47	322.89
k12	89.27	0.43	98.62	62.42	366.32
k13	78.80	0.47	183.78	50.69	309.37
k14	72.64	0.48	201.51	55.87	263.78
k15	78.19	0.53	179.41	215.75	280.90
k16	77.31	0.46	168.23	103.43	301.40
k21	88.13	0.46	190.28	125.00	280.69
k22	64.13	0.47	182.17	55.87	294.83
k23	88.43	0.64	206.75	255.27	283.76
k28	68.00	0.54	161.84	89.74	306.97
k29	86.93	0.42	196.31	108.47	281.51
k30	80.50	0.45	185.93	47.37	297.37
k31	86.85	0.56	186.37	117.57	289.28
k39	82.50	0.38	166.22	99.85	296.05
k40	72.64	0.48	149.14	109.50	326.47
k46	67.00	0.66	37.90	109.36	310.54
k47	61.67	0.39	35.59	50.62	297.55
k48	74.50	0.51	196.90	38.70	269.62
k54	58.67	0.69	55.53	17.04	290.48
k55	55.20	0.57	61.82	14.80	286.78
k61	67.75	0.57	73.56	64.70	286.87
k62	59.43	0.58	106.50	43.41	278.41
k63	63.57	0.46	108.16	19.93	280.27
k71	72.57	0.55	106.69	58.03	266.25
k72	81.00	0.53	118.91	67.70	256.61
k75	70.25	0.41	92.90	21.03	287.87

2.3. Attribute Hierarchical Model (AHM)

As a subjective weighting method, the AHM is an improvement of the AHP. There is no need to calculate the feature vector and perform a consistency test, thus avoiding the shortcomings of the AHP, and so, an AHM is a more practical subjective analysis method. The decision-making steps using AHM are divided into three steps: (1) building a recursive hierarchy, (2) constructing a judgment matrix and calculating the relative weights, and (3) calculating the synthetic weights of the scenarios concerning the system's objectives to make a decision.

The hierarchical model of water inrush risk is constructed from an overlying separation layer, as shown in Figure 6. The flow chart of the evaluation process is shown in Figure 7.

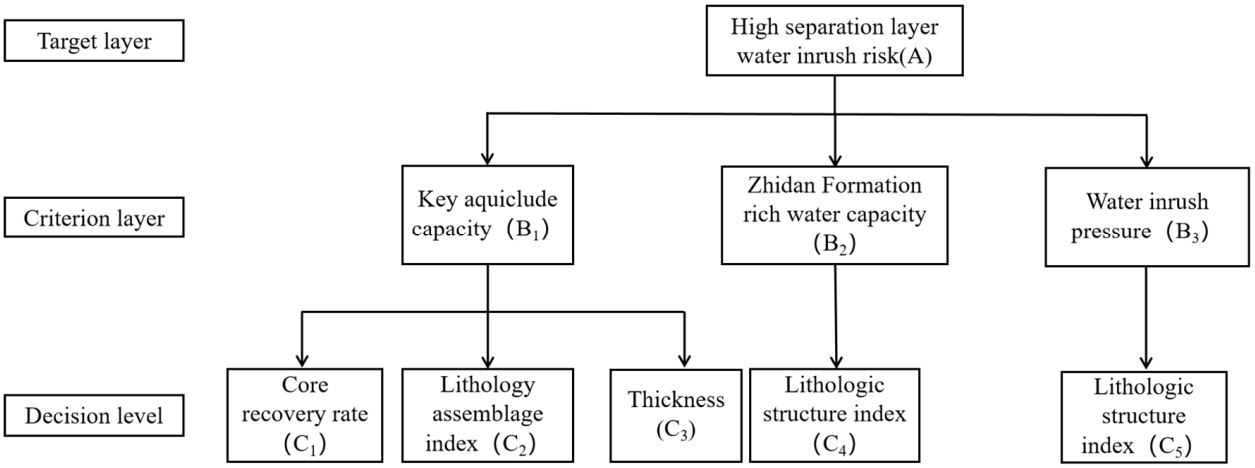

Figure 6. A hierarchical model for the risk of water inrush from an overlying separation layer.

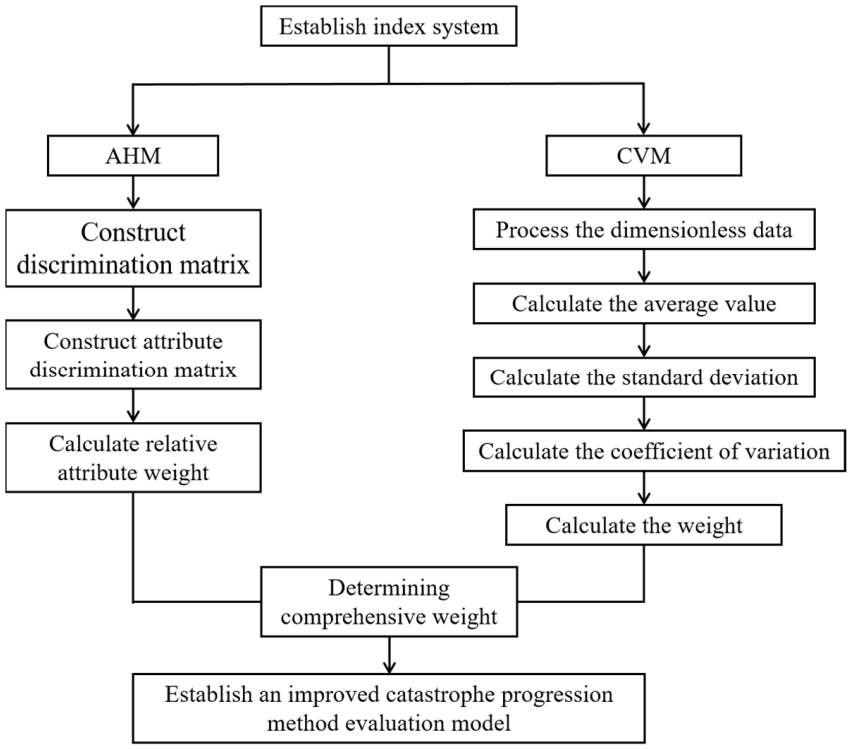

Figure 7. Flow chart of the prediction of water inrush risk.

The Saaty scaling method was adopted to obtain the n-order discriminant matrix $R = (r_{ij})_{n\times n}$ via the expert scoring method, in which R_{ij} represents the importance of factor i compared with factor j. The discriminant matrix $R = (r_{ij})_{n\times n}$ has the following properties:

$$\begin{cases} R_{ij} > 0 \\ R_{ij} = 0 \\ R_{ij} = \frac{1}{k_{ij}} \end{cases} \quad (3)$$

where $i \neq j$, $1 \leq i \leq n$ and $i \leq j \leq n$.

The attribute discrimination matrix was constructed, which can be expressed as follows:

$$k_{ij} = \begin{cases} \frac{2m}{2m+1} & R_{ij} = m,\ i \neq j \\ \frac{1}{2m+1} & R_{ij} = \frac{1}{m},\ i \neq j \\ 0.5 & R_{ij} = 1,\ i \neq j \\ 0 & R_{ij} = 1,\ i \neq j \end{cases} \tag{4}$$

where m is a positive integer not less than 2.

The relative attribute weight of each indicator was constructed, which can be expressed as follows:

$$\omega_{AHM} = \frac{2}{n(n-1)} \sum_{j=1}^{n} k_{ij} \tag{5}$$

where $i = 1, 2, \ldots, n$, n is the number of evaluation indicators.

2.4. Coefficient of Variation Method (CVM)

As an objective evaluation method, the CVM is usually based on the standard deviation of each index's data and the average quotient to obtain a method to measure the degree of variation among the indicators. When the value of a certain index is more different in terms of the overall index data, it means that the index plays a greater role in the evaluation of the overall goal and can be given a greater weight. In contrast, the weight is smaller. Equations (6) and (7) were used to carry out dimensionless processing on the positive correlation index and negative correlation index of the original matrix, respectively, and then the mean Equation (8), standard deviation Equation (9) and coefficient of variation Equation (10) were calculated successively to obtain the weight of each index.

The dimensionless data were processed via the following steps.

For the positive correlation index, k_{ij} can be calculated as follows:

$$k_{ij} = \frac{x_{ij} - \min\limits_{j}(x_{ij})}{\max\limits_{j}(x_{ij}) - \min\limits_{j}(x_{ij})} \tag{6}$$

For the negative correlation index, k_{ij} can be calculated as follows:

$$k_{ij} = \frac{\max\limits_{j}(x_{ij}) - x_{ij}}{\max\limits_{j}(x_{ij}) - \min\limits_{j}(x_{ij})} \tag{7}$$

The average value of each index can be expressed as follows:

$$\overline{\chi_j} = \frac{1}{n} \sum_{i=1}^{m} \chi_{ij} \tag{8}$$

The standard deviation of each index can be expressed as follows:

$$D = \sqrt{\frac{1}{n} \sum_{i=1}^{m} (\chi_{ij} - \overline{\chi})^2} \tag{9}$$

The coefficient of variation of each index can be expressed as follows:

$$\delta_j = \frac{D}{\overline{\chi_{\mathrm{j}}}} \tag{10}$$

The weight of each index can be expressed as follows:

$$\omega_j = \frac{\delta_j}{\sum\limits_{j=1}^{n} \delta_j} \tag{11}$$

Among them, $\sum_{j=1}^{n} \omega_j = 1$.

2.5. Catastrophe Progression Method (CPM)

The CPM method is an important application of catastrophe theory to evaluation systems. It is an evaluation method with fuzzy function characteristics derived from catastrophe theory and calculus [26]. Zhang et al. [27] predicted the risk of coal and gas explosions in coal mines using the catastrophe progression method. Compared with the commonly used multi-index comprehensive evaluation methods at the present stage, the calculation complexity of the CPM is relatively small, and the operation is simpler. It considers the relative importance of the indicators. It uses the normalized formula to calculate the indicators, solving the problems that the indicators cannot be quantified and the complex calculation procedures. Therefore, it is generally applicable to the study of evaluation index systems.

2.5.1. Determining the Catastrophe Type of Each System of Indicators

In the CPM, according to the number of variables controlled by basic factors, there are four commonly used catastrophe types, including folding catastrophes, pointy catastrophes, dovetail catastrophes and butterfly catastrophes, as shown in Table 5 below.

Table 5. The four catastrophe models.

Type of Catastrophe	Control Variable	State Variable	Potential Function
Folding	1	1	$f(x) = x^3 + \mu x$
Pointy	2	1	$f(x) = x^4 + \mu x^2 + \nu x$
Dovetail	3	1	$f(x) = x^5 + \mu x^3 + \nu x^2 + \omega x$
Butterfly	4	1	$f(x) = x^6 + \mu x^4 + \nu x^3 + \omega x^2 + tx$

According to the catastrophe theory, through simultaneous equations $f(x)'$ and $f(x)''$, the normalized formula for each catastrophe type was derived, as shown in Table 6 below.

Table 6. Normalized value of catastrophe progression method.

Type of Catastrophe	Control Variable	State Variable	Normalized Formula
Folding	1	1	$x\mu = \sqrt{\mu}$
Pointy	2	1	$xu = \sqrt{u}, xv = \sqrt[3]{v}$
Dovetail	3	1	$xu = \sqrt{u}, xv = \sqrt[3]{v}, xw = \sqrt[4]{w}$
Butterfly	4	1	$xu = \sqrt{u}, xv = \sqrt[3]{v}, xw = \sqrt[4]{w}, xt = \sqrt[5]{t}$

2.5.2. Nondimensionalization of the Raw Data

In the application of the CPM, the value range of control variables should be 0–1. Therefore, dimensionless processing should be carried out on the original data to nondimensionalize the index.

2.5.3. Evaluation with the Normalized Formula

The catastrophe progression of each level should follow the complementary and noncomplementary principles, that is, when there is a correlation between the subordinate indicators, the complementary principle is adopted, and the catastrophe progression of the upper level is the normalized average of the subordinate indicators; otherwise, the noncomplementary principle is adopted, and the catastrophe progression of the upper level is the minimum value of the normalized value of the subordinate indicators. The Pearson correlation coefficient method was used to determine the correlation between each index, and the following Equation (12) was adopted:

$$r = \frac{\sum_{i=1}^{m} (x_i' - \overline{x})(y_i' - \overline{y})}{\sqrt{\sum_{i=1}^{m} (x_i' - \overline{x})^2} \sqrt{\sum_{i=1}^{m} (y_i' - \overline{y})^2}} \quad (12)$$

where m represents the number of samples; x_i' and y_i' represent standardized index values; $\overline{x}$ and $\overline{y}$ represent the mean value of indicators after standardization; and r is the correlation coefficient. When r is greater than or equal to 0.8, it indicates that the two indicators are highly correlated; $0.8 > r \geq 0.5$ indicates a moderate correlation; when $0.5 > r \geq 0.3$, the correlation is low; and $r < 0.3$ indicates little correlation.

3. Results

3.1. Weight Determination via the AHM

The discriminant matrix R is obtained according to the expert scoring method, and the results are shown in Tables 7 and 8.

Table 7. Discriminant matrix R (A–B_i, i = 1, 2, 3).

Evaluation Index	B_1	B_2	B_3
B_1	1	5	3
B_2	1/5	1	1/3
B_3	1/3	3	1

Table 8. Discriminant matrix R (B_1–Ci, i = 1, 2, 3).

Evaluation Index	C_1	C_2	C_3
C_1	1	3	4
C_2	1/3	1	3
C_3	1/4	1/3	1

According to Equation (4) above, the attribute discrimination matrix K was calculated using scale R_{ij}, and the results are shown in Tables 9 and 10.

Table 9. Attribute discriminant matrix K (A–B_i, i = 1, 2, 3).

Evaluation Index	B_1	B_2	B_3
B_1	0	10/11	6/7
B_2	1/11	0	1/7
B_3	1/7	6/7	0

Table 10. Attribute discriminant matrix K (B1–C_i, i = 1, 2, 3).

Evaluation Index	C_1	C_2	C_3
C_1	0	6/7	8/9
C_2	1/7	0	6/7
C_3	1/9	1/7	0

According to Equation (5), the relative attribute weight ω_{AHM} of the factors influencing the risk of water inrush in the upper layer was calculated, and the results are shown in Table 11.

Table 11. AHM analytic hierarchy process to calculate index weights.

Influencing Factors	C_1	C_2	C_3	C_4	C_5
Attribute weight ω_{AHM}	0.0498	0.1962	0.3427	0.08	0.33

3.2. Coefficient of Variation Method to Determine the Weight

According to Equation (6) through to Equation (11), the original data were calculated, and the weight values of each index of the risk of water inrush in the upper layer were obtained, as shown in Table 12.

Table 12. Coefficient of variation method to calculate index weight.

Influencing Factors	C_1	C_2	C_3	C_4	C_5
Index weight ω_j	0.1800	0.1559	0.2067	0.2930	0.1644

3.3. Determine the Weight Ranking of Comprehensive Indicators

The following Equation (13) was used to combine the subjective weight value calculated via AHM and the objective weight value calculated via the CVM to obtain the comprehensive weight ω_i of each influencing factor:

$$\omega_i = \alpha\omega_{AHM} + (1 - \alpha)\omega_j \quad (13)$$

where α is the preference coefficient, which represents the degree of preference of the analyzer and judge of the influencing factors in terms of the proportion of subjective weight in the comprehensive weight. In this paper, the value is 0.7 after considering the practical significance of the evaluation system of the risk of water inrush in the upper layer. The comprehensive weight of each factor was obtained, as shown in Table 13 below.

Table 13. Comprehensive weight value of influencing factors.

Influencing Factors	C_1	C_2	C_3	C_4	C_5
Index weight ω_i	0.08886	0.18411	0.3019	0.1439	0.28032

The ranking results of comprehensive indexes were as follows: the thickness of the aquiclude C_3, the hydrostatic head of the Zhidan Formation C_5, the lithologic assemblage index of the aquiclude C_2, the lithologic structure index of the Zhidan Formation C4 and the core recovery rate from the aquiclude C_1.

3.4. Establish an Improved Catastrophe Progression Method Evaluation Model

The core recovery rate C_1, lithologic assemblage index C_2 and thickness of the aquiclude C_3 can be used to composite a dovetail catastrophe. The lithologic index of the Zhidan Formation C_4 can be used to composite a folding catastrophe. The hydrostatic head of the Zhidan Formation C_5 can be used to composite a folding catastrophe. The water-retaining capacity of key layer B1, water-retaining capacity of the Zhidan Formation B_2 and water inrush pressure B3 can be used to composite the dovetail catastrophe.

Equations (6) and (7) above were used to process the original data and the standardized data were obtained, as shown in Table 14.

The correlation coefficient matrix of indicators was obtained by calculating the original data in Table 14 according to Formula (11), as shown in Table 15 below.

Table 14. Standardization of indicator data.

Borehole	C_1	C_2	C_3	C_4	C_5
S01	0.9123	0.3316	0.1369	0.0151	0.3298
S03	0.4629	0.1186	0.3380	0.1211	0.6716
S04	0.7858	0.1541	0.2775	0.1179	0.4779
S05	0.7652	0.0000	0.4884	0.2353	0.8064
S07	0.6369	0.4099	0.4076	0.8069	0.6179
S09	0.6341	0.6068	0.2783	0.7395	0.4647
S10	0.3180	0.4661	0.2617	0.8793	0.4490
S13	0.4482	0.3786	0.0000	0.5564	0.0000
S15	0.5891	0.3833	0.8457	0.9401	0.5225
S16	0.5422	0.1575	0.7850	0.3718	0.4331
S18	0.7652	0.0586	0.8793	0.2044	0.4228
N18	0.3770	0.3901	0.6234	0.0800	1.0000
N42	0.6537	0.3045	0.3775	0.0161	0.8150
N19	0.4042	0.2460	0.4587	0.0476	0.8347
N46	0.3099	0.3822	0.4399	0.4421	0.7287
N47	0.2868	0.5213	0.3150	0.8241	0.4647
N51	0.7197	0.7187	0.7575	0.0598	0.3056
N56	0.0080	0.2621	0.9085	0.4952	0.7349
N58	0.3553	0.3024	0.4262	0.9094	0.6391
k3	0.4448	0.4137	0.1151	0.8977	0.4830
k7	0.1327	0.6803	0.5815	0.0554	0.8227
k8	0.4273	0.4554	0.2221	0.0402	0.6225
k12	0.0000	0.3366	0.6520	0.1981	0.9960
k13	0.3074	0.4321	0.1820	0.1493	0.5062
k14	0.4881	0.4603	0.0841	0.1708	0.1142
k15	0.3253	0.5833	0.2061	0.8357	0.2614
k16	0.3512	0.4179	0.2678	0.3686	0.4377
k21	0.0337	0.4193	0.1461	0.4583	0.2596
k22	0.7381	0.4283	0.1908	0.1708	0.3812
k23	0.0248	0.8714	0.0551	1.0000	0.2860
k28	0.6243	0.6260	0.3031	0.3117	0.4856
k29	0.0688	0.3212	0.1128	0.3895	0.2667
k30	0.2575	0.3950	0.1701	0.1354	0.4031
k31	0.0711	0.6703	0.1677	0.4274	0.3335
k39	0.1988	0.2055	0.2789	0.3537	0.3917
k40	0.4881	0.4599	0.3731	0.3938	0.6533
k46	0.6537	0.9169	0.9872	0.3932	0.5163
k47	0.8102	0.2434	1.0000	0.1490	0.4046
k48	0.4336	0.5438	0.1095	0.0994	0.1644
k54	0.8983	1.0000	0.8899	0.0093	0.3438
k55	1.0000	0.6893	0.8552	0.0000	0.3120
k61	0.6317	0.7034	0.7904	0.2075	0.3128
k62	0.8759	0.7257	0.6086	0.1190	0.2400
k63	0.7543	0.4033	0.5994	0.0213	0.2560
k71	0.4902	0.6559	0.6075	0.1798	0.1354
k72	0.2428	0.5993	0.5401	0.2200	0.0525
k75	0.5583	0.2924	0.6836	0.0259	0.3214

Table 15. Correlation coefficients between indicators.

	C_1	C_2	C_3	C_4	C_5
C_1	1.0000				
C_2	0.0308	1.0000			
C_3	0.3743	0.0838	1.0000		
C_4	−0.3654	0.0705	−0.2559	1.0000	
C_5	−0.1528	−0.3434	0.2174	−0.0369	1.0000

As seen from the data in Table 15, the relationship among indicators is either a weak correlation or noncorrelation, which meets the principle of non-complementarity. Therefore, the principle of taking the minimum value is adopted. The results of the water inrush risk from an overlying separation layer calculated using borehole data are shown in Table 16.

Table 16. Numerical calculation results of water inrush hazard risk from an overlying separation layer.

Borehole	A	Borehole	A	Borehole	A	Borehole	A
S01	0.5919	N42	0.5967	k14	0.5384	k46	0.8898
S03	0.7009	N19	0.6833	k15	0.6737	k47	0.8081
S04	0.7258	N46	0.6512	k16	0.7193	k48	0.5752
S05	0	N47	0.7491	k21	0.6182	k54	0.5575
S07	0.799	N51	0.7032	k22	0.6609	k55	0.5523
S09	0.7263	N56	0.5469	k23	0.4845	k61	0.8215
S10	0.7152	N58	0.6733	k28	0.7419	k62	0.7663
S13	0	k3	0.5824	k29	0.5795	k63	0.6182
S15	0.8522	k7	0.6965	k30	0.6421	k71	0.7166
S16	0.7348	k8	0.6692	k31	0.6398	k72	0.6119
S18	0.6231	k12	0	k39	0.7267	k75	0.6334
N18	0.7292	k13	0.6531	k40	0.7815		

The natural breakpoint method is a method that classifies the dataset according to the discontinuous places in the dataset. According to the natural breakpoint method, the risk level of water inrush in the overburden is divided into three levels, namely, 0–0.7 is the safe zone, 0.7–0.8 is the transition zone and 0.8–0.9 is the danger zone; thus, a zoning diagram of water inrush risk in the overburden is established. The areas with a high risk of water inrush are mainly concentrated in the southern part of the mining area, while the risk in the northern area is relatively small (Figure 8).

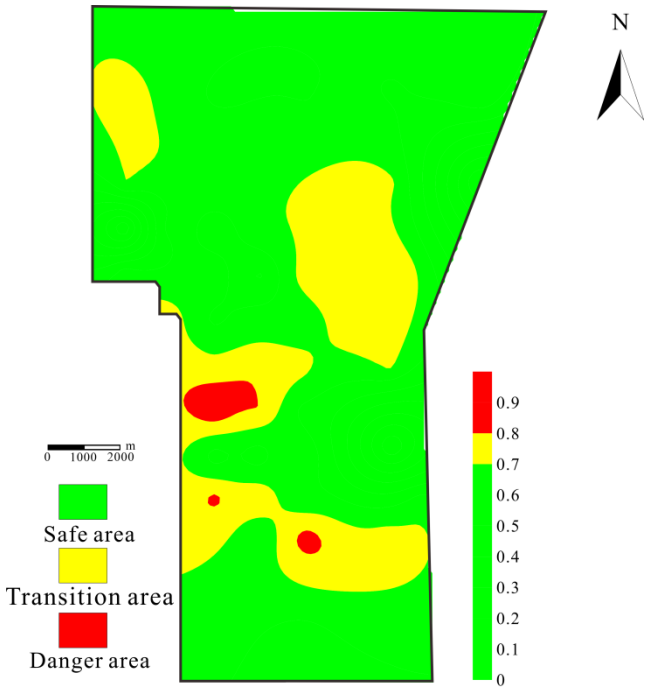

Figure 8. Prediction map of the overlying water inrush hazard zones.

4. Conclusions

(1) The core recovery rate, lithologic assemblage index, key aquiclude thickness, hydrostatic head and lithologic structure index of the Zhidan Formation are selected as

the basis for studying of the water inrush from an overlying separation layer. A risk prediction model based on combination weighting and an improved catastrophe progression method is constructed to predict the risk of water inrush from the overlying separation layer of the double-layer structure in the 221 mining area of Shilawusu coal mine.

(2) This paper applies the subjective and objective weighting method to improve the evaluation index locally. Then, the typical sample of high water inrush risk levels is established. To a certain extent, it reduces the disadvantage of difficult weight allocation caused by complex water inrush disaster factors, enriches the evaluation and research system of water inrush risk prediction and has great significance for avoiding the threat of water inrush from the separation layer.

(3) Due to the complexity of the induced mechanism and disaster factors of overlying separation layer water inrush, the quantification and weight determination of indicators still need to be discussed and studied. In addition, the indicators selected in this paper and the risk prediction of overlying separation layer water inrush are all based on the Shilawusu coal mine, and more robust data need to be collected for the whole mining area and the critical parameters of the mathematical model for further discussion.

Author Contributions: All authors contributed to the study conception and design. Writing—review and editing, D.X.; Investigation, C.H.; Writing—original draft, Z.D.; Formal analysis, J.H. and J.Y.; Visualization, J.W. All authors have read and agreed to the published version of the manuscript.

Funding: This research was financially supported by the National Natural Science Foundation of China (Grant No. 41702305).

Conflicts of Interest: On behalf of all authors, the corresponding author states that there are no conflict of interest.

References

1. Wang, M.-J.; Yu, D.-H. Simulation of water hazards caused by burst of cells formed by overburden stratum separation. *Chin. J. Geotech. Eng.* **2010**, *32*, 231–236. (In Chinese)
2. He, J.-H.; Li, W.-P.; Qiao, W. A rock mechanics calculation model for identifying bed separation position and analyzing overburden breakage in mining. *Arab. J. Geosci.* **2020**, *13*, 920. [CrossRef]
3. Li, H.; Chen, Q.; Shu, Z.; Li, L.; Zhang, Y. On prevention and mechanism of bed separation water inrush for thick coal seams: A case study in China. *Environ. Earth Sci.* **2018**, *77*, 759. [CrossRef]
4. Qiao, W.; Wang, Z.W.; Li, W.P.; Lv, Y.G.; Li, L.G.; Huang, Y.; He, J.H.; Li, X.Q.; Zhao, S.L.; Liu, M.N. Formation mechanism, disaster-causing mechanism and prevention technology of roof bed separation water disaster in coal mines. *J. China Coal Soc.* **2021**, *46*, 507–522. (In Chinese)
5. Gui, H.; Lin, M.; Song, X. Features of separation water hazard in China coalmines. *Water Pract. Technol.* **2017**, *12*, 146–155. [CrossRef]
6. Yan, H.; He, F.; Yang, T.; Li, L.; Zhang, S.; Zhang, J. The mechanism of bedding separation in roof strata overlying a roadway within a thick coal seam: A case study from the Pingshuo Coalfield, China. *Eng. Fail. Anal.* **2016**, *62*, 75–92. [CrossRef]
7. He, J.H.; Li, W.P.; Liu, Y.; Yang, Z.; Liu, S.L.; Li, L.F. An improved method for determining the position of overlying separated strata in mining. *J. Eng. Fail. Anal.* **2018**, *83*, 17–29. [CrossRef]
8. Hu, R.; Wu, J.; Zhai, X.; Liu, W. Recognition and Prevention of Bed Separation Water: Based on Trapezoid Platform Model. *Geofluids* **2021**, *2021*, 6626268. [CrossRef]
9. Ji, Y.; Cao, H.; Zhao, B. Mechanism and Control of Water Inrush from Separated Roof Layers in the Jurassic Coalfields. *Mine Water Environ.* **2021**, *40*, 357–365. [CrossRef]
10. Wu, L.; Bai, H.; Ma, D. Prediction and Prevention of Water Inrush Hazards from Bed Separation Space. *Mine Water Environ.* **2021**, *40*, 657–670. [CrossRef]
11. Gui, H.; Tong, S.; Qiu, W.; Lin, M. Research on preventive technologies for bed-separation water hazard in China coal mines. *Appl. Water Sci.* **2018**, *8*, 7. [CrossRef]
12. Gui, H.; Lin, M.; Song, X. Identification and Application of Roof Bed Separation (Water) in Coal Mines. *Mine Water Environ.* **2018**, *37*, 376–384. [CrossRef]
13. Wang, Z.; Zhang, Q.; Shao, J.; Zhang, W.; Wu, X.; Zhu, X. New type of similar material for simulating the processes of water inrush from roof bed separation. *J. ACS Omega* **2020**, *5*, 30405–30415. [CrossRef]
14. Wang, Z.; Zhang, Q.; Zhang, W. A novel collaborative study of abnormal roof water inrush in coal seam mining based on strata separation and wing crack initiation. *Eng. Fail. Anal.* **2022**, *142*, 106762. [CrossRef]

15. Li, L.; Shu, Z.-Y.; Feng, Y.-F. Analysis and prevention on mechanism of water inrush from bed separation water of overburden by fully-mechanized top coal caving mining in ultra thick seam. *Coal Sci. Technol.* **2018**, *46*, 175–182. (In Chinese) [CrossRef]
16. Xie, D.; Han, J.; Zhang, H.; Wang, K.; Du, Z.; Miao, T. Risk Assessment of Water Inrush from Coal Seam Roof Based on Combination Weighting-Set Pair Analysis. *Sustainability* **2022**, *14*, 11978. [CrossRef]
17. Yuan, S.; Sui, W.; Han, G.; Duan, W. An optimized combination of mine water control, treatment, utilization, and reinjection for environmentally sustainable mining: A case study. *J. Mine Water Environ.* **2022**, *41*, 828–839. [CrossRef]
18. Zhu, T.; Li, W.; Chen, W. Risk assessment of Cretaceous water inrush in the Ordos Basin based on the FAHP-EM. *Water Policy* **2021**, *23*, 1249–1265. [CrossRef]
19. Li, B.; Wu, Q.; Meng-yu, C. Risk analysis model of water inrush through the seam floor based on set pair analysis. *J. Mine Water Environ.* **2018**, *37*, 281–287.
20. Yuan, S.; Sun, B.; Han, G.; Duan, W.; Wang, Z. Application and Prospect of Curtain Grouting Technology in Mine Water Safety Management in China: A Review. *Water* **2022**, *14*, 4093. [CrossRef]
21. Fan, G.; Zhang, S.; Zhang, D.; Zhang, C.; Chen, M.; Li, Q. An Index of Aquiclude Destabilization for Mining-Induced Roof Water Inrush Forecasting: A Case Study. *Water* **2019**, *11*, 2170. [CrossRef]
22. Li, L.; Xie, D.; Wei, J.; Yin, H.; Li, G.; Man, X.; Zhang, W. Analysis and control of water inrush under high-pressure and complex karstic water-filling conditions. *Environ. Earth Sci.* **2020**, *79*, 493. [CrossRef]
23. Zhang, P.; Zhu, H.; Wu, Y.; Duan, Z.; Niu, H.; Li, F. State-of-the-art of mechanism of water inrush from bed separation and key technology of prevention and pre-control in China. *J. Eng. Geol.* **2021**, *29*, 1057–1070. (In Chinese)
24. Li, Z.; Wang, Y.; Liu, S.-Q. Analysis of influence factors on rock quality designation and core recovery percentage. *J. Min. Sci. Technol.* **2017**, *2*, 511–518. (In Chinese)
25. Hou, E.K.; Tong, R.J.; Wang, S.J.; Feng, J.; Chen, T. Prediction method for the water enrichment of weathered bedrock based on Fisher model in Northern Shaaxi Jurassic coalfield. *J. China Coal Soc.* **2016**, *41*, 2312–2318. (In Chinese)
26. Tian, L.-G.; Hu, Q.-Y. Study on the Influencing Factors of Ecological-Health in Small Watershed by Catastrophe Progression Method. *Yellow River* **2020**, *42*, 71–75 + 80. (In Chinese)
27. Zhang, T.J.; Ren, S.X.; Li, S.G.; Zhang, T.C.; Xu, H.J. Application of the catastrophe progression method in predicting coal and gas outburst. *Min. Sci. Technol.* **2009**, *19*, 430–434. [CrossRef]